

The Inner Coma and Nucleus of Comet Hale–Bopp: Results from a Stellar Occultation

Yanga R. Fernández and Dennis D. Wellnitz

Department of Astronomy, University of Maryland, College Park, Maryland 20742-2421

E-mail: yan@astro.umd.edu

Marc W. Buie, Edward W. Dunham, Robert L. Millis, Ralph A. Nye, John A. Stansberry, and Lawrence H. Wasserman

Lowell Observatory, 1400 W. Mars Hill Road, Flagstaff, Arizona 86001

Michael F. A'Hearn and Carey M. Lisse

Department of Astronomy, University of Maryland, College Park, Maryland 20742-2421

Meg E. Golden and Michael J. Person

Department of Earth, Atmospheric and Planetary Sciences, Massachusetts Institute of Technology, Cambridge, Massachusetts 02139-4307

Robert R. Howell

Department of Physics and Astronomy, University of Wyoming, P.O. Box 3905, University Station, Laramie, Wyoming 82071

and

Robert L. Marcialis and Joseph N. Spitale

Lunar and Planetary Laboratory, University of Arizona, Tucson, Arizona 85721

Received January 21, 1998; revised February 10, 1999

We discuss the properties of the nucleus and inner coma of Comet Hale–Bopp (C/1995 O1) as derived from observations of its occultation of Star PPM 200723 on 5 October 1996, while the comet was 2.83 AU from the Sun. Compared to previous occultations by active comets, this is possibly the closest to the nucleus one has ever observed. Three chords (lightcurves) through the comet's inner coma were measured, though only one chord has a strong indication of measuring the occultation, and that was through thin cirrus. We have constrained the radius of the nucleus and properties of the coma using a simple model; there is a large valid section of parameter space. Our data show the optical depth of the coma was ≥ 1 within 20 to 70 km of the center of the (assumed spherical) nucleus, depending on the coma's structure and the nucleus' size. The dependence of the dust coma's opacity on cometocentric distance, ρ , was steeper than expected for force-free, radial flow, being probably as steep as or steeper than $1/\rho^{1.4}$ within 100 km of the nucleus (though it is marginally possible to fit one coma hemisphere with a $1/\rho$ law). Assuming the dust coma flowed radially from a spot at the center of the nucleus and that the coma's profile was not any steeper than ρ^{-2} , the upper limit to the radius of the nucleus is about 30 km, though relaxing these assumptions limits the radius to 48 km. The chord through the coma does not show the same coma structure within

100 km of the nucleus as that which is apparent in larger-scale (~ 700 km/pixel) imaging taken just before the event, suggesting that (a) the star's path sampled the acceleration region of the dust, and/or (b) azimuthal variation in the inner coma is different than that seen in the outer coma. © 1999 Academic Press

Key Words: Comets; Hale–Bopp.

I. INTRODUCTION

Although about 10^3 comets have been discovered throughout history, the ensemble properties of the population of the cometary nuclei remain elusive. Measurements have been made of a few dozen (Meech 1999), but confident and unambiguous knowledge exists for only a handful of objects (A'Hearn 1988, Belton 1991). Moreover, most of these objects are of short-period; knowledge about the nuclei of long-period comets is even more limited. Information on physical characteristics beyond the simple properties (e.g., size and rotation) exists only for the nucleus of 1P/Halley. The typically large geocentric distance during a cometary apparition (~ 1 AU), the typically small size

of the nucleus itself (~ 0.1 to 10 km), and the obscuring effects of the coma are the primary reasons for this lack of knowledge. The high resolution necessary to observe the heart of the comet usually prohibits the study of the inner coma itself on scales of a few tens of kilometers.

Stellar occultations, on the other hand, hold great promise for probing the nuclei and deep inner comae of comets (see, e.g., Combes *et al.* 1983), though there have been only a few published reports, and the chords have not come particularly close to the nuclei. The extinction has been found to be a few percent at a distance of several hundred kilometers from the nucleus for comets of various activity levels and dust-to-gas ratios (e.g., Larson and A'Hearn 1984, and Lecacheux *et al.* 1984); a factor of four reduction in starlight was apparently measured in Comet Burnham (C/1959 Y1; Dossin 1962). Bus *et al.* (1996) report the observation of a star's complete disappearance behind the centaur (2060) = 95P/Chiron, but the low activity, large nucleus, and regular orbit of this "comet" mark this as a special case. Though most previous data on cometary occultations were obtained at permanent observatories, with a sufficient number of portable telescope systems spaced across a territory over which an occultation is predicted to occur, as we have done here, one can in principle obtain an estimate of the opacity structure of the coma and hence learn about the dynamics and scattering properties of the dust. The likelihood of witnessing the occultation of a star by the nucleus itself would also be increased with a sufficiently fine grid of observers.

It is worthwhile to emphasize the differences between observing asteroid and comet occultations. While an asteroid is a point source, located near the center of brightness, and usually on a well-defined path (making the prediction uncertainty just a few shadow widths), a cometary nucleus is often swamped by coma emission of an uncertain morphology, making it hard to decide where exactly the nucleus is within the comet image's brightest pixel. (This is especially true for Hale-Bopp, the dustiest comet on record.) Moreover nongravitational forces push the comet away from the ephemeris position (though fortunately this is probably not a problem for Hale-Bopp). There are even potentially significant errors built in to the ephemeris itself, since it is usually derived from astrometry of the comet's brightest spot, not the nucleus' location. Lastly the typical comet nucleus is only a few kilometers wide. The result is to make observing comet occultations more logistically difficult than their asteroid counterparts.

Here we report the observation of the dimming of Star PPM 200723 (=SAO 141696 = BD -04°4289 = GSC 5075-0004) from its occultation by Comet Hale-Bopp (C/1995 O1). Barring a terrestrial explanation, the star's light was completely or nearly completely blocked along part of one occultation chord, implying that a line of sight through an optically thick portion of the inner coma, or through the nucleus itself, was observed. On two other chords, no significant diminution of light was observed. If our interpretation is correct, this is the closest to the nucleus a typical comet has ever been sampled via a stellar oc-

cultation. We give results from analyses of the data from this unique observation.

II. OBSERVATIONS

The circumstances of the 5 October 1996 (UT) event are given in Table I. The occultation path (uncertain to ± 60 s in time and ± 700 km in distance) passed thru the western United States soon after sunset on 4 Oct. Six portable teams were arrayed across the region (crossed squares in Fig. 1) for the observations; one permanent facility was also used. Table II lists the location, equipment, and data obtained by the seven teams. Originally the teams were to spread out from central Nevada northward to maximize the chance that at least one team would record a significant optical depth ($\geq 10\%$) through the coma; clouds covering Washington, Oregon, Idaho, and western Montana during the event dictated where each portable team positioned itself. Sufficient signal during the event was obtained only by Teams 5, 6, and 7: Team 5 recorded a feature that appears to be the event itself, through passing cirrus clouds; Team 6 has at best a marginal lightcurve feature at the appropriate time; and Team 7 did not detect the event.

The three solid lines in Fig. 1 trace out two 100-km wide swaths which show the last preevent prediction of the occultation track. The true track was only as wide as Hale-Bopp's nucleus (with projection effects), and the swaths do *not* represent the systematic error in the determination of the track's location, which were closer to ± 700 km (1σ). These swaths were used to aid in choosing locations for the portable teams.

TABLE I
Characteristics of Comet Hale-Bopp Occultation

• The star, PPM 200723	
Magnitude ^{a,b}	$m_V = 9.1$
MK spectral type ^b /luminosity class ^c	K0V
J2000 right ascension ^b	17 ^h 29 ^m 59 ^s .845
J2000 declination ^b	-4°48'09".45.
• The comet, C/1995 O1 (Hale-Bopp)	
Magnitude (in 24-arcsec wide circular aperture)	$m_R = 8.5$
Heliocentric distance	2.83 AU
Geocentric distance	3.00 AU
Distance scale at comet	2.18 km \pm 10 ⁻³ arcsec
Solar elongation	71.0°
Phase	19.5°
Proper motion and PA	8.41 arcsec/h, 30.6°
Equivalent linear speed	5.11 km/s
• The observing locale ^d	
Time of mid-event	5 Oct 1996, 03:17:48 UT \pm 3 s
Speed of nuclear shadow	11.6 km/s
Elevation and azimuth of comet	25.8°, 235.8°

^a Smithsonian Astrophysical Observatory 1966.

^b Röser and Bastian 1991.

^c Measured by Jeffrey Hall of Lowell Observatory (private communication).

^d Specifically, location of Team 5 (see Table II) at the time of event.

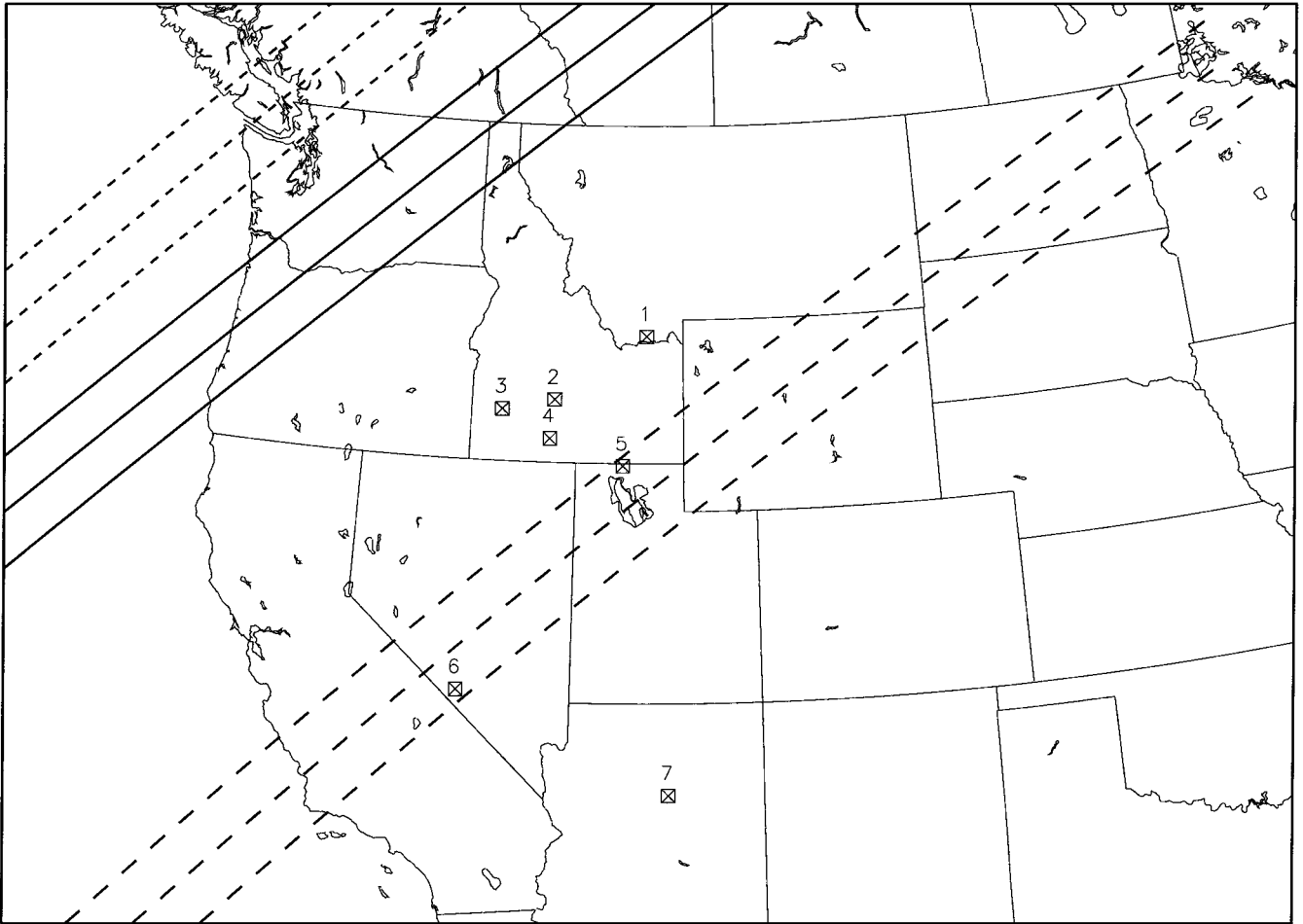


FIG. 1. Map of the western United States showing the locations of the participating teams as listed in Table II (crossed squares), and the occultation track predictions: long-dashed lines show the original ephemeris prediction; short-dashed lines show intermediate solution including astrometric corrections; solid lines show last prediction including corrections from deriving the nucleus' position within the comet's photocenter. See text for details. The three lines mark out a 200-km wide swath, which was used for planning purposes; the nucleus' shadow is much narrower.

The preevent ephemeris (Solution 41 by D. K. Yeomans of Jet Propulsion Laboratory) predicted an occultation path shown by the long-dashed lines in Fig. 1. Astrometric corrections to this, using images of the comet taken with the U. S. Naval Obser-

vatory Flagstaff Station (USNOFS) 1.5-m telescope, moved the track to the short-dashed lines in Fig. 1. A coma-fitting technique (Lisse *et al.* 1999b) was employed to find the source of the coma (i.e., the nucleus) within an image of the comet's

TABLE II
Observations of Occultation by Comet Hale-Bopp

Team	Location	System ^a		Summary of results
		CCD	PMT	
1. Buie and Golden	44°39' N 112°05' W	✓		Heavy clouds; data exist but not during event.
2. Dunham and Stansberry	43°19' N 114°41' W	✓		Heavy clouds; data exist but not during event.
3. Nye and Person	43°05' N 116°19' W	✓		Heavy clouds; no data.
4. Marcialis and Spitale	42°30' N 114°47' W	✓		Heavy clouds; no data.
5. Wellnitz and Fernández	41°57' N 112°44' W		✓	Thin clouds; data show detection of event.
6. Wasserman and Howell	37°12' N 117°00' W		✓	Clear; data show marginal detection of event?
7. Millis	35°06' N 111°32' W		✓	Clear; data show no detection of event.

^a Teams 1 through 6 used Celestron C14 14-in (0.35-m) telescopes; Team 7 used the Lowell Observatory 31-in (0.8-m) NURO telescope. Teams checked under "CCD" used a charge-coupled device. Teams checked under "PMT" used a photomultiplier tube with effective wavelength near 4000 Å.

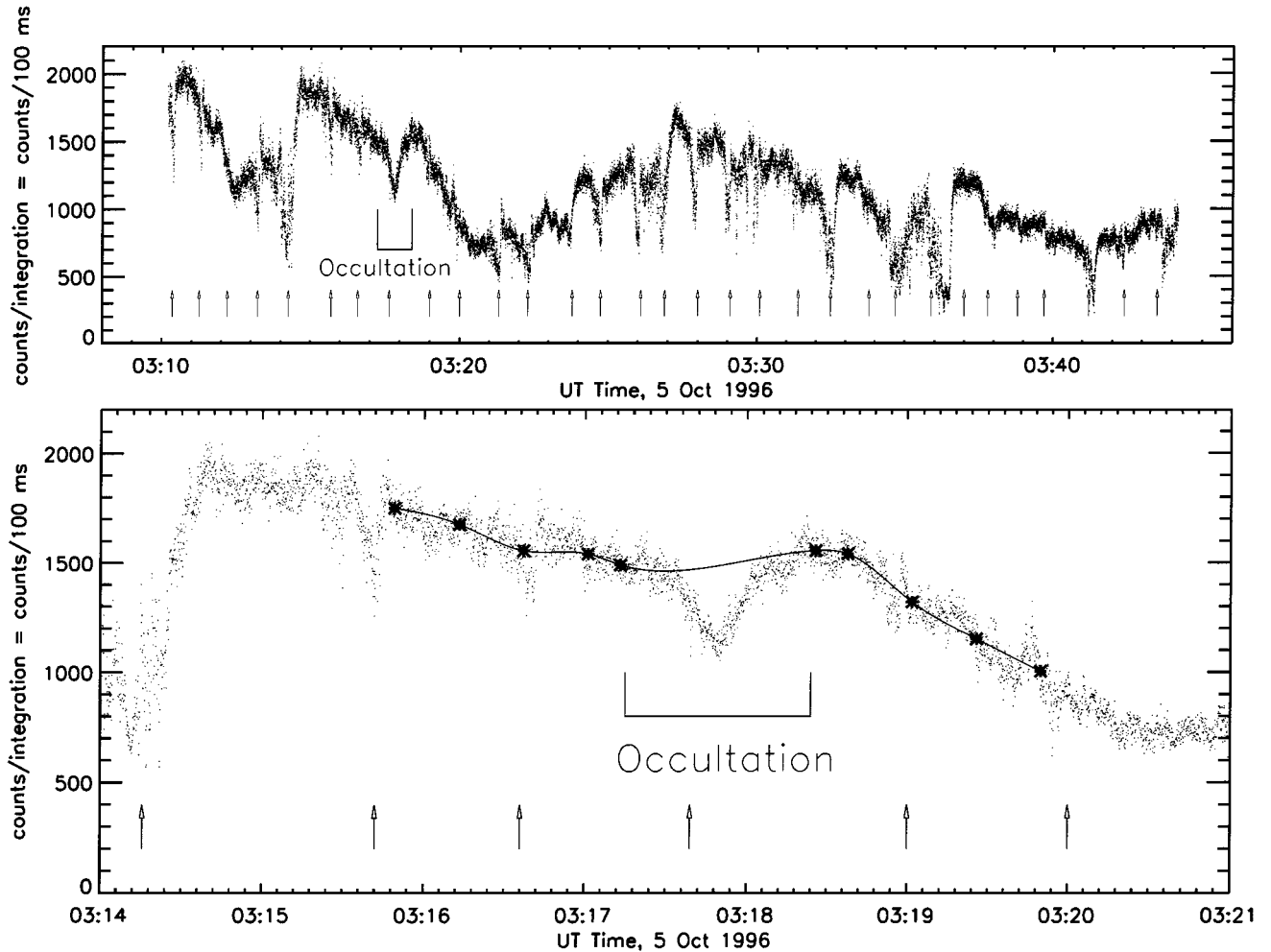


FIG. 2. Lightcurve from Team 5 showing the occultation event, a feature that is morphologically distinct from all others. Top plot covers all 34 min of the lightcurve; bottom shows 7 min centered on the occultation feature. Integration time for each data point was 100 ms. Arrows indicate tracking corrections; see text for details. The tracking correction near the center of the occultation was not significant. The asterisks indicate the locations where the large-scale effect of the passing cirrus clouds was sampled, and the thick line is a spline fit to those points. This fit was used by our model to grossly account for the nonphotometric conditions.

center of brightness, moving the track to the solid lines in Fig. 1. The corrections gave a net shift to the prediction of Yeomans' ephemeris of about 9×10^2 km northwest. Our apparent detection of the nucleus occurred closer to the original prediction than the corrected one, indicating we had underestimated the prediction errors and that our corrections did not reduce the error, only delimit it. As we will show, with all the uncertainties of event prediction (as mentioned in Section I), the detection of the occultation ~ 800 km away from the "best" guess is perfectly reasonable.

Weather and equipment problems prevented Team 5 from observing the comet and the star separately to determine their relative brightnesses in the photometer passband. Using the known spectral characteristics of both objects, combined with broad- and narrowband imaging taken near the day of the event, we estimate the star to be 0.35 ± 0.02 times as bright as the sum of

the comet, sky flux, and detector noise. The method is described in the Appendix.

The lightcurve from Team 5 is shown in Fig. 2. The data span about 34 min (top graph); the ~ 7 min centered on the time of deepest occultation (at 03:17:48 UT ± 3 s) are shown in the lower panel. The photometer integrations were 100 ms long, and the aperture was circular and one arcminute wide.

The lightcurve is characterized by (a) long (several minutes), gradual changes in the count rate due to passing clouds (e.g., the general trend from 03:14:30 to 03:27:30); (b) precipitous drops in flux due to the comet and star (which were nearly superimposed) being near the edge of the aperture, immediately followed by even more rapid (few seconds) rises as the target is restored to the center of the field of view (e.g., at 03:26 and 03:27:45); (c) small drops in flux due to the comet and star moving a bit off-center in the aperture, followed by a quick restoration as

the target is recentered (e.g., at 03:11:30, 03:16:30, 03:19:00, 03:20:00, and (importantly) at 03:17:35); and (d) the occultation event itself near 03:17:48. The distinct morphological differences between these four types give us confidence that we have observed the occultation event. The occultation caused a fairly symmetric valley in the lightcurve of about one minute in length, shorter than the time scale for the effects of passing clouds, but longer than the time scale for a drop and rise in flux due to the position of the target in the aperture.

Cases (b) and (c) above were caused by the telescope not exactly tracking at the proper motion rate of the comet. The times of these corrections are marked with arrows in Fig. 2. The correction at 03:17:35, the one before it, and the two after were all minor and belong to case (c). Since most of the comet's flux was in its coma, a slight offset of the target did not cause a significant decrease in flux; the more obvious manifestations of these corrections are the small noise spikes from the telescope drive's electrical interference.

The drop in count rate at the time of deepest occultation is about 25%, which is consistent with the star being totally blocked from view, since it was 0.35 times the brightness of the other contributors to the flux ($0.35/1.35 \approx 25\%$). Moreover it occurs close to the predicted time of 03:18:10 for the location of Team 5. The dip could not be due to a jet contrail since the lightcurve would resemble a profile through a uniform density gas cylinder, which would have a shallower slope through the middle of the event, unlike what has been recorded. While we cannot unambiguously rule out that an unusual cloud passed in front of the comet, the circumstantial evidence does imply an observation of the occultation.

There is a dip in the lightcurve at approximately 03:12:30 UT which may be interpreted as morphologically distinct from the effects of both clouds and tracking errors, and so could be construed to be the occultation event; it is the only other feature in the lightcurve, aside from that at 03:17:48 UT, that could have been caused by the occultation. An event this early would, however, imply a rather large error of thousands of kilometers. While it is possible to model the circumstances of the event (in the manner described in the next section) to reproduce the curve, the fits are less robust than those for the 03:17:48 feature. Accounting for the effects of extinction by the clouds makes the feature quite skew, which reduces the ability of our model to adequately fit it.

In sum, due to the unique shape of the feature at 03:17:48, our ability to model it well, its closeness to the predicted time, and its depth, we believe that it is likely due to the occultation event and not due to tracking errors or clouds.

The lightcurve recorded by Team 6 is shown in the top of Fig. 3, observed from a position 643 km farther along the shadow track from Team 5, and 170 km perpendicular to it. This lightcurve was obtained in a cloudless sky so all variations are due to tracking errors, gain changes, and manifestations of the occultation. At the time one would expect the comet's shadow to pass over Team 6 (based on Team 5's results; marked on the figure),

there is a drop in flux of a few percent (lower panel of Fig. 3). That feature's shape is similar to other tracking error corrections in the lightcurve, so it is not clear if this is the occultation. However, it does allow us to limit the opacity of the coma 170 km from Team 5's chord at 8%.

III. ANALYSIS

a. Model and Assumptions

Our model for the lightcurve assumes the optical depth, τ , is proportional to the inverse of the cometocentric distance, $1/\rho$, raised to a constant power n . (The steady-state, force-free, radially flowing dust coma would have $n=1$.) As the comet passes between Earth and the star, the attenuation of starlight will depend on time. A schematic of the scenario is given in Fig. 4. Ignoring clouds for the moment, we express each point in the lightcurve, $S(t)$, as a constant term (S_0 , the comet's flux plus sky flux and detector noise) plus a term representing the star's flux times the attenuation factor ($e^{-\tau(t)}$). Let $C = 0.35 \pm 0.02$ be the ratio of the star's unattenuated flux to S_0 . Then $S(t) = S_0(1 + Ce^{-\tau(t)})$. If the comet's nucleus itself passes between the star and Earth, the flux during that interval will just be S_0 . If the star disappears behind the nucleus at time t_i , and reappears at time t_o , then the lightcurve can be represented by

$$S(t) = \begin{cases} S_0(1 + Ce^{-\tau_i(t)}), & \text{if } t < t_i; \\ S_0, & \text{if } t_i < t < t_o; \text{ and} \\ S_0(1 + Ce^{-\tau_o(t)}), & \text{if } t > t_o. \end{cases} \quad (1)$$

Since we do not assume *a priori* that the two sides of the coma that are sampled by the inbound and outbound sections of the occultation are the same, we have a three-piece function. We can however remove the nuclear chord in the model simply by setting $t_i = t_o$. The subscript *i* denotes a quantity related to the ingress, *o* to the egress.

Evaluating τ as a function of time requires knowing ρ . The distance from the center of the nucleus at a given time t is just $\sqrt{b^2 + (v(t - t_m))^2}$, where b is the impact parameter, v is the speed of the comet across the sky, and t_m is the time of mid-occultation. Since the center of the (assumed spherical) nucleus does not have to be the coordinate origin for ρ , we include an extra term, l_0 , that describes the offset (parallel to the star's direction of motion) of the coordinate origin from the nuclear center.¹ Thus, $\rho(t) = \sqrt{b^2 + (v(t - t_m) - l_0)^2}$ and the optical depth is

¹ The impact parameter b was *not* used as a measure of the offset from the coordinate origin in the perpendicular direction. The coordinate origin always lies on the horizontal line in Fig. 4 that runs through the center of the nucleus. There is no evidence that our assumption is justified but it made the modeling tractable and allowed us to constrain properties of the nucleus.

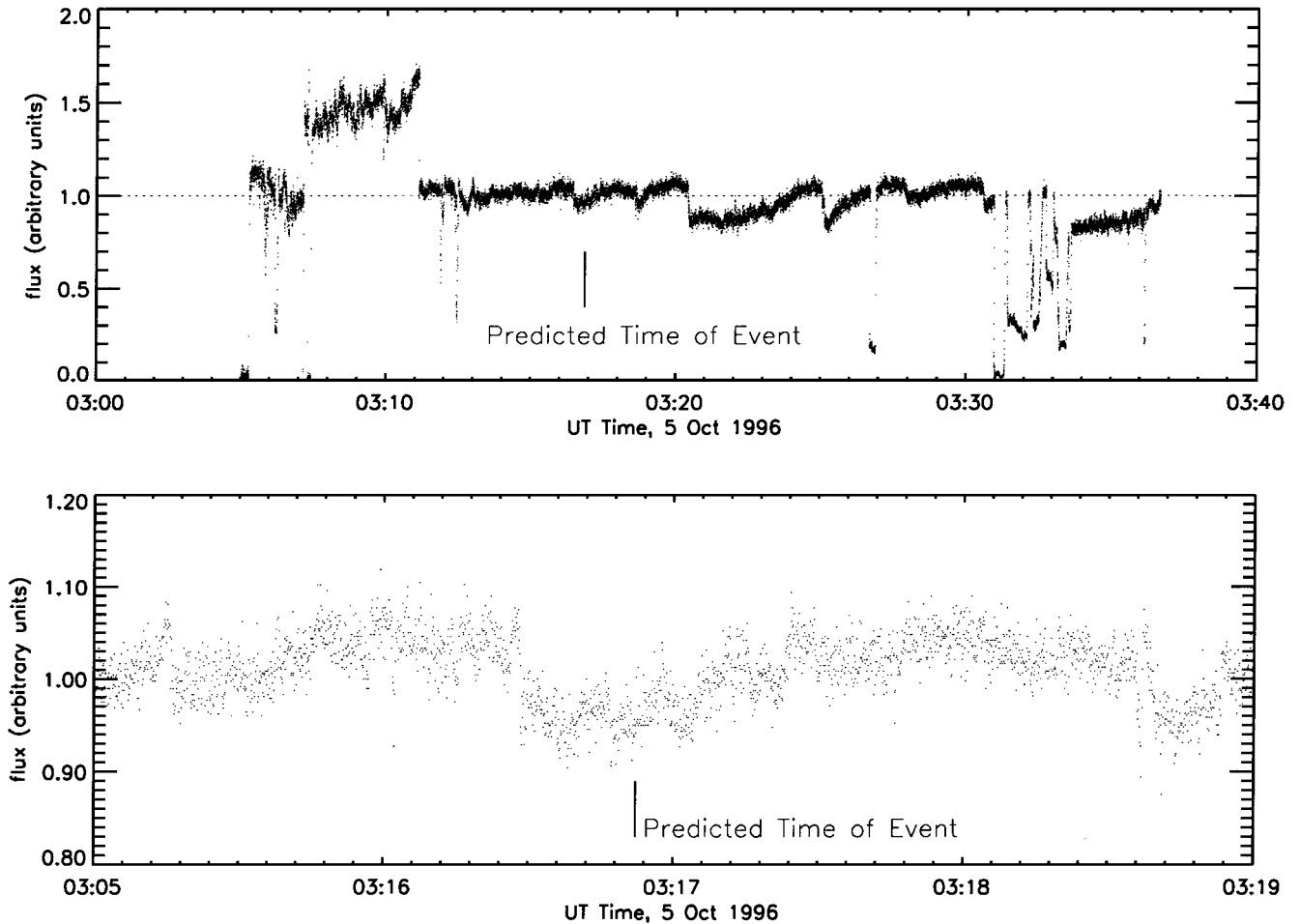


FIG. 3. Lightcurve from Team 6, with the expected time of occultation marked (based on the time of deepest occultation recorded by Team 5). Top panel shows the whole curve; lower panel shows a close-up of the most relevant section. Ordinate units are arbitrary. There is a slight dip in the count rate at the appropriate time, but it is not distinguishable from other, comparably shaped features.

given by

$$\tau_i(t) = \left(\frac{\kappa_i}{\sqrt{b^2 + (v(t - t_m) - l_{0i})^2}} \right)^{n_i}, \quad (2a)$$

$$\tau_o(t) = \left(\frac{\kappa_o}{\sqrt{b^2 + (v(t - t_m) - l_{0o})^2}} \right)^{n_o}, \quad (2b)$$

where κ is the length scale of the opacity. Since we allow the time t_m to be fit by the model, we have overparameterized the lateral shift in the coordinate origin; the best parameter to quote really is $\sum l_0 \equiv l_{0i} + l_{0o}$, i.e., the separation of the two coordinate origins. In later discussion we will mention the nuclear radius, R , which is just

$$R = \sqrt{b^2 + \left(\frac{1}{2}l_n\right)^2} \equiv \sqrt{b^2 + \left(\frac{1}{2}v(t_o - t_i)\right)^2}, \quad (3)$$

i.e., the square root of the quadrature-addition of the impact

parameter and half the length of the chord through the nucleus. A listing of all quantities is given in Table III.

In addition to this theoretical model, we accounted for the large-scale extinction in the lightcurve due to clouds near the time of the event by multiplying our model by an empirical function. In Fig. 2, the asterisks in the lightcurve indicate where it was sampled to estimate the clouds' effect. The thick line is a spline fit through those points and represents the empirical function. We sampled the cloud's effect outside the region to which we applied our model. The observation site of Team 5 was dark and moonless, so the clouds would only cause extinction of the starlight, not increase the sky brightness.

We have made some assumptions to simplify the fitting. The spherical nucleus assumption immediately implies that $t_o - t_m = t_m - t_i$. Also note that our model coma (Fig. 4) is not perfectly circular; n and κ can be different between the two hemispheres, but within one hemisphere they cannot vary. We have not included in our fitting the data near the time of the tracking correction (2.8 s centered at 03:17:45.9 UT), and two brief noise spikes (0.5 s starting at 03:17:39.0 UT; 1.3 s starting at 03:17:52.8 UT; see

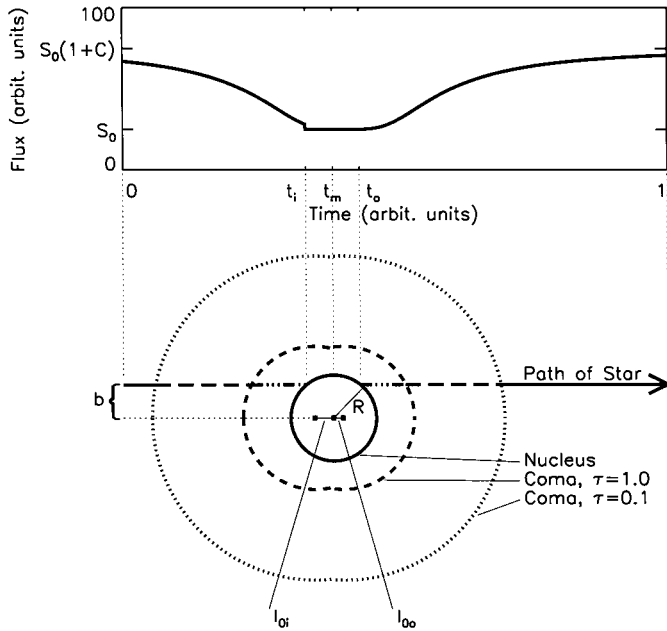


FIG. 4. Not-to-scale schematic of the occultation scenario. Top plot shows a generic lightcurve based on the star’s passage behind the coma and nucleus of the comet (arrow, in bottom of figure). Times of the beginning and end of nuclear chord are marked (t_i and t_o , respectively), as is mid-occultation (t_m); note the abrupt jump in the flux at time t_i as the star passes behind the nucleus. The locations of a coma opacity of 0.1 and 1.0 are marked. All variables are defined in Table III.

Fig. 2). Lastly, we have assumed that the radius of the nucleus is no bigger than 50 km. Analysis of high-resolution mid-infrared, microwave, and optical imaging of the comet have constrained the nuclear size to be smaller than this value (Wink 1999, Y. R. Fernández *et al.* in preparation, Weaver and Lamy 1999), so our assumption allows for a large error in these works. In terms of our fitting, this means we will not consider models that require a combination of b and l_n such that $R \geq 50$ km.

Further assumptions were made about the physical environment of the coma. First, we assumed that n could be no larger

than 2.4. Hydrodynamic models of the coma (Divine 1981) imply that a steepening of the dust density profile to the equivalent of ρ^{-3} (yielding a surface brightness (and opacity) proportional to ρ^{-2}) can occur within a few nuclear radii of the nucleus. Others (e.g., Gombosi *et al.* 1983, 1985; Marconi and Mendis 1983, 1984) have also used dusty-hydrodynamic models to calculate dust velocities and/or number densities as a function of cometocentric distance, and their results do show some steepening of the dust profile within a few nuclear radii of the surface. From these works we conjecture that the tenable limit to n in this phenomenon is ~ 2 to $2\frac{1}{2}$, though the higher values have less theoretical support. Again, we allow for a large error in these previous works. Our second assumption is that l_0 cannot be so large as to extend off the near edge of the nucleus itself. In other words, we did not allow the case where $\rho = 0$ (and the divergence of the opacity) could be encountered by the star.

b. Results of Model Fitting

Since there are so many data points, in this case the χ^2 statistic is useful only as a coarse indicator of “good” and “bad” fits; e.g., a fit that goes through all of the points but is too shallow to cover the lightcurve’s minimum could have a reduced χ^2 (χ_R^2) of just 1.15, which would still be beyond the 99% confidence level for the 620-odd degrees of freedom. The best way to ascribe a “good” fit is by eye, with χ^2 being a rough guide. There are three morphological characteristics that must be satisfied for a fit to be considered “good”: (a) it must be sufficiently deep to cover the valley at 03:17:48 UT (determined by κ , n , b , and to some extent by $t_o - t_i$); (b) it must follow the shape of the valley’s walls (from 03:17:33 to 03:17:45 and from 03:17:53 to 03:18:03 UT; determined by κ , n , and l_0); and (c) it must lie on the median value of the wings (from 03:17:15 to 03:17:33 and from 03:18:03 to 03:18:22 UT; determined by κ and n). We say “median” because we do not attempt to fit the small jumps in flux that occur in the wings; these may be due to clouds or to real opacity features in the comet’s coma. A given model was

TABLE III
Parameters of the Model of Nuclear and Comatic Structure

Symbol	Description	Value
S_0	Count rate from comet + sky + dark current	Fit
C	Ratio of count rate from star to S_0	0.35 ± 0.02
Subscript i, o	Indicates variable pertains to ingress and egress of occultation, respectively	NA
τ_i, τ_o	Opacity	Calculated
t_i, t_o	Beginning and ending times of occultation by nucleus	Fit
t_m	Time of mid-event	Fit
l_n	Length of the nuclear chord of the occultation	Fit
b	Impact parameter	Fit
v	Speed of comet across sky	5.11 km/s
n_i, n_o	Exponent of the power-law profile of the opacity	Fit
κ_i, κ_o	Length scale of the opacity	Fit
l_{oi}, l_{oo}	Distance of cometocentric coordinate origin from center of nucleus	Fit
R	Nuclear radius	Calculated

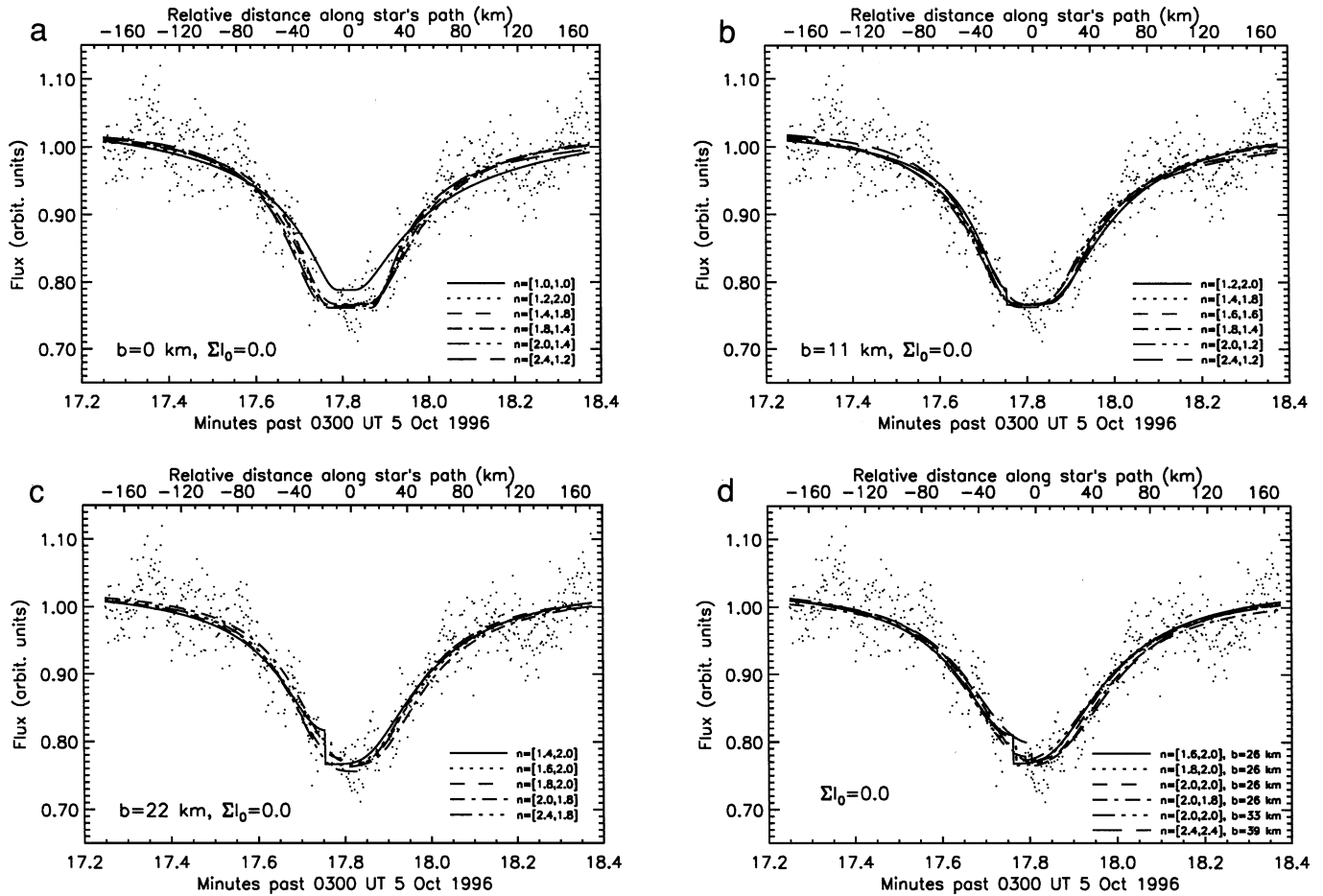


FIG. 5. (a–d) Examples of combinations of parameters that provide “good” fits (as defined in the text) to the Team 5 lightcurve. These are *not* meant to be an exhaustive portrayal of the entire valid parameter space, but only to demonstrate how well the curve can be fitted. All models presented here assume there was no nuclear chord. Each plot has the impact parameter b written within its borders. The first four plots assume $\sum l_0 \equiv l_{0i} + l_{0o} = 0.0$. Each plot shows five or six models with varying n_i and n_o (written as $n = [n_i, n_o]$). Plot (a) shows clearly that $n_i = n_o = 1.0$ does not fit the curve; plot (d) shows an example of an impact parameter higher than ~ 35 km that marginally fits the curve. The blank section near 17.7 min past 0300 UT, caused by a tracking correction, allows for great latitude in the kind of models that can fit the data. (e–h) Same as for (a–d), except the four plots allow $\sum l_0 \neq 0.0$, and each model mentions the value used.

detuned with the various parameters until the fit could no longer be considered marginally “good.”

The results of the fitting are summarized in Table IV. We have explored parameter space using $b = 0, 6.5, 11, 22, 26, 33, 39,$ and 45 km (and higher values, but it turned out that they never sufficiently fit the lightcurve), and $n = 0.8, 1.0, 1.2, 1.4, 1.6, 1.8, 2.0,$ and 2.4 . Entries in the table give values or ranges for the quantities $\kappa_i, \kappa_o,$ and l_n that yield “good” or marginally “good” fits as defined above. (In the “Comments” column, the presence or absence of “m” indicates a marginally good or good fit.) All fits listed in the table have $0.96 \leq \chi_R^2 \leq 1.05$, with most around $0.97, 0.98,$ or 0.99 . With only one chord through the comet showing unambiguous extinction, the valid parameter space offered by our model is large. Moreover, the unfortunate location of the tracking correction so close to the valley of the lightcurve, thus removing those data points, allows an even wider valid space.

Figure 5 displays representative fits to our lightcurve. It is not meant to be as exhaustive as Table IV is, but graphically shows

the large variation in parameter values that still allows adequate fitting. The first four plots have forced $\sum l_0 = 0$, the last four allow it to vary. The value of b is written within each plot. The abrupt jumps in the flux predicted by some models are due to the star passing behind the nucleus; note the jump at time t_i in the schematic lightcurve of Fig. 4. Special note should be taken of one model in Fig. 5a using $n_i = n_o = 1.0$; it cannot fit the curve. Also, Fig. 5d shows a model with $b = 39$ km; such a high impact parameter allows only a marginal fit to the curve. The value of χ_R^2 is 1.0 in all but the one obviously incorrect model, where it is 1.2.

We mention some other notable results from the modeling:

- Our modeled constraints on b limit the nucleus’ radius R (via Eq. 3) to ≤ 48 km. Restricting ourselves to the best (not marginal) fits and to $n \leq 2.0$, then $R \leq 30$ km.
- For completeness we modeled the case where $b = 0$ and $l_n = 0$, even though clearly this is an unphysical scenario.

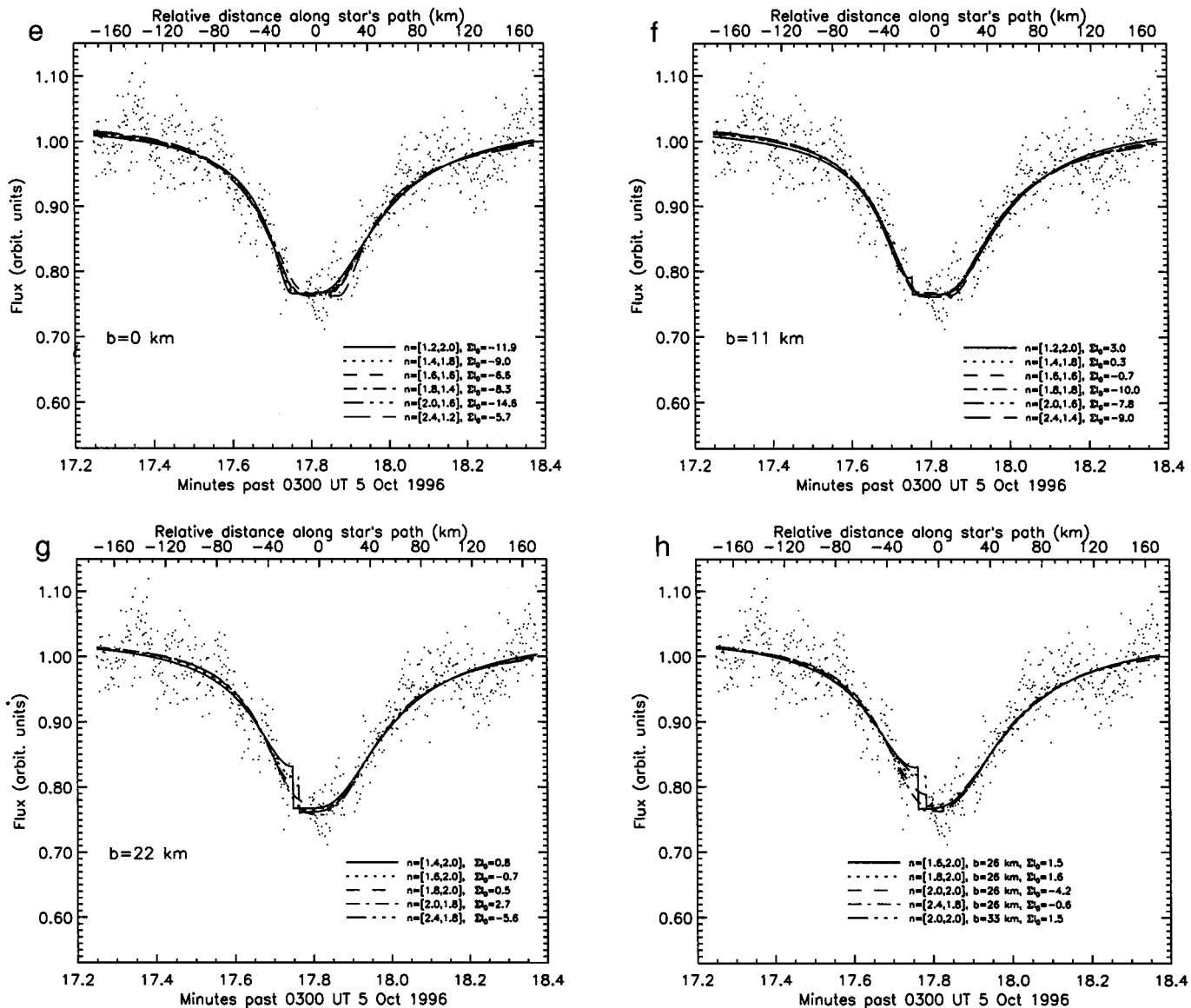


FIG. 5—Continued

Fortunately, it was never the case that the lightcurve was significantly better fit with $l_n = 0$ than with $l_n > 0$.

- The distance from the coordinate origin to the $\tau = 1$ point in the coma is given by κ . For some models in Table IV $R > \kappa$, so the maximum coma opacity is less than unity. (The fit to the lightcurve for these models requires the nuclear chord to pass through the bad-data gaps.) On the other hand with a small R the maximum opacity can be as high as 2. Note that the noise in the lightcurve prevents us from confidently distinguishing between $\tau = 2$ and $\tau > 2$ (or $\tau = \infty$).

- For clarity we have not put in the allowable ranges of κ for each model in Table IV. Typically changing κ by ± 3 km still yields a good or marginally good fit.

- The acceptable fits to the lightcurve require n to be at least 1.0, though the fits are slightly better as n increases. Further, if

$n \leq 1.2$ in one hemisphere, then $n \geq 2.0$ in the other. This steepness to the coma is opposite the sense found in *Giotta* images of Comet Halley's inner coma, where $n < 1$ as $\rho \rightarrow R$ due to localized sources of dust on the surface (Thomas and Keller 1990, Reitsema *et al.* 1989). We postulate that the steepness in Hale-Bopp's coma is due to azimuthal structure (where we have assumed none) and/or to the passage of the star's path through the acceleration region of the dust. Clearly our model is simplistic, but the lack of data does not justify using a more complex formulation.

- One power law can satisfy the constraints of the lightcurves measured by both Team 5 and Team 6 if, in general, $n \geq 1.6$. A letter "c" in the "Comments" column of Table IV indicate which models are consistent with both curves. Furthermore, if we force the coma to be consistent, it is impossible for the nuclear shadow

TABLE IV
Constraints on Parameters to Occultation Model

b (km)	n_i	n_o	κ_i (km) ^a	κ_o (km) ^a	$\rho(\tau = 0.1)$ (km) ^b	$\frac{1}{1 - e^{-\tau}}$ ^c	l_n range (km) ^d	R range (km) ^e	Comments ^f
0	1.0	1.8	21	64	[157,188]	0.40	0–26	0–13	m
0	1.0	2.0	19	66	[155,190]	0.39	0–22	0–11	
0	1.0	2.4	16	67	[153,174]	0.36	0–15	0–8	
0	1.2	1.8	25	61	[159,185]	0.41	0–24	0–12	m
0	1.2	2.0	23	60	[159,185]	0.38	0–24	0–12	
0	1.2	2.4	20	62	[135,159]	0.35	0–24	0–12	m, c
0	1.4	1.6	32	53	[166,179]	0.44	0–40	0–20	m
0	1.4	1.8	32	54	[162,179]	0.42	0–40	0–20	
0	1.4	2.0	28	55	[143,175]	0.38	0–36	0–18	c
0	1.6	1.2	45	40	[179,166]	0.48	0–52	0–26	m
0	1.6	1.4	43	44	[177,168]	0.47	0–56	0–28	
0	1.6	1.6	38	47	[158,172]	0.44	0–55	0–23	m
0	1.8	1.2	50	37	[179,161]	0.48	0–42	0–21	m
0	1.8	1.4	43	42	[154,168]	0.46	0–45	0–23	
0	1.8	1.6	42	42	[149,168]	0.43	0–54	0–27	m, c
0	2.0	1.0	54	30	[172,157]	0.49	0–30	0–15	m
0	2.0	1.2	52	34	[164,159]	0.48	0–34	0–17	c
0	2.0	1.4	45	39	[142,166]	0.45	0–48	0–24	c
0	2.0	1.6	44	39	[137,166]	0.43	0–48	0–24	m, c
0	2.4	1.0	55	27	[142,157]	0.48	0–25	0–13	m, c
0	2.4	1.2	53	29	[140,157]	0.46	0–27	0–14	m, c
0	2.4	1.4	52	30	[135,154]	0.44	0–30	0–15	m, c
6.5	1.0	1.8	22	67	[155,190]	0.39	0–15	0–10	m
6.5	1.0	2.0	19	68	[153,192]	0.37	0–15	0–10	
6.5	1.2	1.6	26	60	[160,186]	0.40	0–28	0–15	m
6.5	1.2	1.8	26	61	[160,186]	0.39	0–25	0–14	
6.5	1.2	2.0	23	63	[155,188]	0.36	0–25	0–14	m
6.5	1.4	1.4	37	50	[170,175]	0.43	0–47	0–24	m
6.5	1.4	1.6	34	53	[168,177]	0.42	0–46	0–24	
6.5	1.4	1.8	32	55	[163,179]	0.39	0–41	0–22	
6.5	1.4	2.0	27	57	[137,181]	0.36	0–36	0–19	m, c
6.5	1.6	1.4	43	44	[177,168]	0.44	0–55	0–28	m
6.5	1.6	1.6	38	48	[161,172]	0.41	0–54	0–28	
6.5	1.6	1.8	35	50	[147,175]	0.39	0–46	0–24	m
6.5	1.8	1.0	56	33	[188,158]	0.49	0–33	0–18	m
6.5	1.8	1.2	52	35	[185,160]	0.41	0–35	0–19	
6.5	1.8	1.4	47	39	[167,163]	0.36	0–45	0–23	c
6.5	1.8	1.6	42	43	[150,168]	0.31	0–48	0–25	m, c
6.5	1.8	1.8	39	45	[139,159]	0.27	0–54	0–28	m, c
6.5	2.0	0.8	64	23	[196,149]	0.49	0–15	0–10	m
6.5	2.0	1.0	60	26	[190,151]	0.45	0–18	0–11	
6.5	2.0	1.2	53	32	[168,158]	0.40	0–33	0–18	m, c
6.5	2.4	0.8	64	20	[166,148]	0.47	0–15	0–10	m
6.5	2.4	1.0	62	22	[162,149]	0.44	0–13	0–9	m, c
6.5	2.4	1.2	57	26	[148,153]	0.41	0–19	0–12	m, c
11	1.0	1.8	22	70	[153,192]	0.38	0–15	0–13	m
11	1.0	2.0	20	72	[151,194]	0.37	0–11	0–12	
11	1.2	1.8	25	64	[158,188]	0.38	0–23	0–16	m
11	1.2	2.0	23	65	[155,190]	0.36	0–17	0–14	c
11	1.4	1.6	34	55	[166,179]	0.36	0–35	0–21	m
11	1.4	1.8	31	57	[159,182]	0.38	0–30	0–19	c
11	1.4	2.0	28	59	[145,184]	0.35	0–27	0–17	m, c
11	1.6	1.4	41	45	[174,170]	0.42	0–52	0–28	
11	1.6	1.6	32	55	[136,182]	0.39	0–30	0–19	c
11	1.6	1.8	30	56	[124,184]	0.33	0–28	0–18	m, c
11	1.6	2.0	27	58	[112,182]	0.32	0–22	0–16	m, c
11	1.8	1.2	52	36	[186,160]	0.45	0–34	0–20	m
11	1.8	1.4	48	40	[171,164]	0.37	0–39	0–22	

TABLE IV—Continued

b (km)	n_i	n_o	κ_i (km) ^a	κ_o (km) ^a	$\rho(\tau = 0.1)$ (km) ^b	$\frac{1}{1 - e^{-\tau^c}}$	l_n range (km) ^d	R range (km) ^e	Comments ^f
11	1.8	1.6	43	44	[154,168]	0.40	0–48	0–26	m, c
11	2.0	1.2	53	34	[166,160]	0.44	0–33	0–20	c
11	2.0	1.4	49	37	[156,162]	0.37	0–33	0–20	m, c
11	2.0	1.6	47	39	[147,164]	0.33	0–39	0–22	m, c
11	2.4	1.0	58	28	[152,155]	0.46	0–15	0–13	m, c
11	2.4	1.2	55	31	[142,158]	0.43	0–20	0–15	m, c
11	2.4	1.4	53	31	[138,158]	0.38	0–25	0–17	m, c
22	1.4	2.0	30	66	[157,189]	0.34	0–22	0–25	m, c
22	1.4	2.4	26	72	[134,187]	0.32	0–13	0–23	m, c
22	1.6	1.8	33	62	[141,187]	0.36	0–24	0–25	m, c
22	1.6	2.0	33	63	[138,187]	0.34	0–25	0–25	c
22	1.6	2.4	30	65	[126,168]	0.29	0–19	0–24	m, c
22	1.8	1.6	39	55	[138,180]	0.37	0–35	0–28	m, c
22	1.8	1.8	35	58	[124,185]	0.35	0–35	0–28	c
22	1.8	2.0	31	62	[113,189]	0.33	0–25	0–25	c
22	2.0	1.6	47	47	[149,170]	0.38	0–40	0–30	m, c
22	2.0	1.8	38	54	[121,180]	0.35	0–31	0–27	c
22	2.0	2.0	33	60	[105,187]	0.32	0–21	0–24	m, c
22	2.4	1.6	50	41	[131,165]	0.36	0–25	0–25	c
22	2.4	1.8	43	47	[112,169]	0.34	0–35	0–28	c
22	2.4	2.0	39	51	[102,159]	0.31	0–37	0–29	m, c
26	1.6	2.0	33	69	[139,192]	0.35	0–20	0–28	m, c
26	1.6	2.4	30	72	[125,188]	0.32	0–12	0–27	m, c
26	1.8	1.8	40	60	[141,183]	0.36	0–35	0–31	m, c
26	1.8	2.0	34	65	[123,189]	0.33	0–23	0–28	c
26	1.8	2.4	30	70	[107,183]	0.31	0–11	0–27	m, c
26	2.0	1.8	40	59	[124,183]	0.33	0–29	0–30	m, c
26	2.0	2.0	36	62	[113,187]	0.33	0–24	0–29	c
26	2.0	2.4	31	68	[99,176]	0.30	0–15	0–27	m, c
26	2.4	1.8	45	50	[118,174]	0.34	0–45	0–34	c
26	2.4	2.0	42	53	[108,168]	0.32	0–40	0–33	c
26	2.4	2.4	32	65	[82,170]	0.29	0–15	0–27	m, c
33	2.0	2.0	42	65	[132,186]	0.33	0–27	0–36	m, c
33	2.0	2.4	37	70	[118,182]	0.30	0–17	0–34	m, c
33	2.4	2.0	48	56	[124,177]	0.31	10–30	33–36	c
33	2.4	2.4	38	68	[99,177]	0.30	0–15	0–34	c
39	2.4	2.4	50	63	[131,163]	0.28	10–30	39–42	m, c
45	2.4	2.4	59	64	[153,168]	0.28	15–38	46–48	m, c

^a Error from fitting is ± 3 km.

^b Cometocentric distance at which coma opacity is 0.1. Error from fitting is ± 20 km. Two values are given, one for each hemisphere.

^c Mean value of $1 - e^{-\tau}$ within 100 km of nuclear surface. Error from fitting is about 8%.

^d Range of lengths of nuclear chord that yields an adequate fit. Error from fitting is ± 4 km.

^e Range of possible nuclear radii based on the range of l_n and b .

^f Codes: m = marginally good fit, c = fit is consistent with opacity measured by Team 6.

to have passed between the two teams. That is, if Teams 5 and 6 were on opposite sides of the nucleus, the parameters describing the two sides of the coma sampled by the two teams would have to be different, which is beyond the scope of our modeling. An alternate explanation is that the coma merely does not have the spherical or hemispherical symmetry that is assumed.

• For most models, we find $-10 \text{ km} \leq \sum l_0 \leq 15 \text{ km}$, though for $b > 30 \text{ km}$, the range is only a few kilometers. Moreover, having the coordinate origin of both hemispheres on the ingress side of the nucleus is slightly favored (by a $\leq 2\%$ decrease in

χ_R^2). Note that in Comet Halley, the origin was found to be near the center of the nucleus (Thomas and Keller 1987).

IV. DISCUSSION

a. Astrometry

Our apparent detection of the occultation implies the nucleus was $(8.0 \pm 0.5) \times 10^2 \text{ km}$ on a perpendicular from the last prediction of the nuclear track. Mid-event occurred about 22 s before the predicted time for the location of Team 5, corresponding

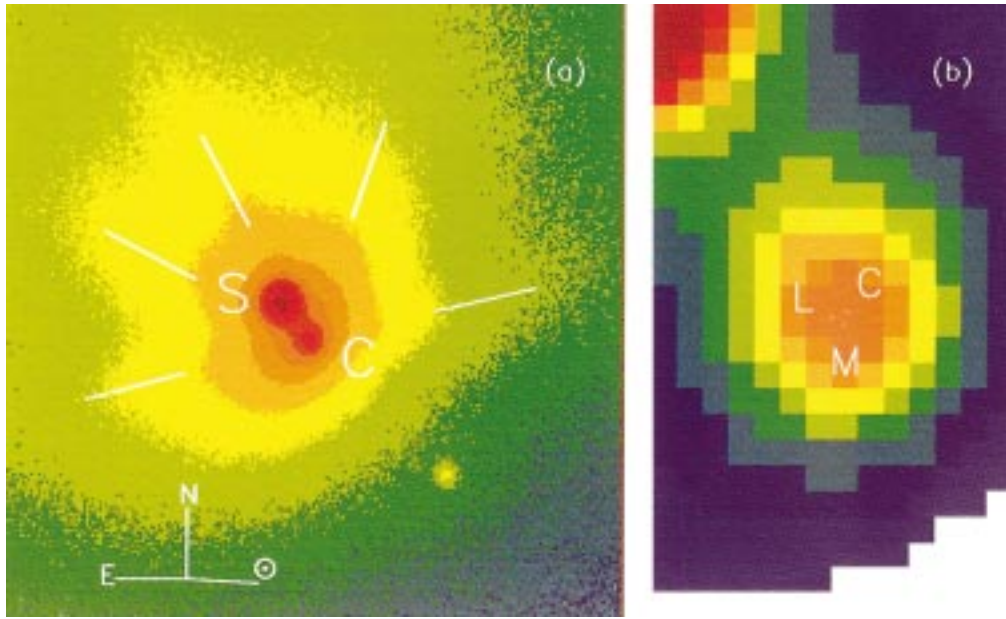


FIG. 6. (a) Image of Comet Hale–Bopp (“C”) and PPM 200723 (“S”) taken less than one hour before the occultation. The scale here is 0.33 arcsec per pixel, corresponding to 720 km of linear distance at the comet; our entire occultation event marked in Fig. 2 covers about one-half of a pixel. Line segments indicate the most prominent jets in the comet’s coma, and show that on ingress the star was traveling along a jet’s edge. (b) Expanded view of the central pixels of the comet. The middle of the brightest pixel, “M”; centroid of brightness, “C”; inferred position from coma-fitting technique of Lisse *et al.* (1999b), “L”.

to 255 km along the track. Considering the errors involved with the prediction, this is not an unacceptably large offset, as we now explain.

Figure 6a shows an image of the comet and star taken one hour before the event (from the USNO Flagstaff Station 1.5-m telescope). Figure 6b, showing an expanded view of the central pixels of the comet, is marked with the middle of the brightest pixel (“M”), the location of the centroid of brightness (“C”), and the estimated position of the nucleus using the coma-fitting technique of Lisse *et al.* (1999b) (“L”; ± 0.25 pixel). The pixel size for the images in Fig. 6 is 0.33 arcsec (7.2×10^2 km at the comet). Our astrometry of the comet’s offset from the ephemeris position (using three nights of USNO images, as mentioned in Section II) was uncertain to 0.3 arcsec (6.5×10^2 km), i.e., almost one pixel. Combined with the uncertainty from the coma-fitting technique, this gives an 1σ error of about 7×10^2 km. So it is quite reasonable to expect the nuclear shadow to have passed over a team several hundred kilometers from the predicted center line.

Our constraint on the location of the nucleus is reasonably consistent with 1998 calculations for the orbit of Hale–Bopp (Donald Yeomans, private communication). However it should be noted that we are estimating the error with respect to the measured position of the comet from the astrometry, not from the ephemeris. Had we used a different ephemeris, say, one that was thought to be more accurate, the only difference would have been to change the offsets measured via the astrometry of the USNO images. We would have arrived at the same prediction and the same observing strategy. Hence, a post-facto ephemeris,

which might be used to try to pin down exactly how far Team 5 was from the nucleus’ shadow, would not make much difference. In essence, our astrometry provided a truer prediction of the comet’s position than any ephemeris would have. Astrometric measurements from post-event imaging would have helped but these data were not taken.

b. Nucleus

As mentioned, we assumed that the nucleus has $R \leq 50$ km, but our fitting further constrains this number, to 30 km, by making two reasonable assumptions. Only marginally good fits are found for models with R much bigger than this, up to 48 km, i.e., almost up to the assumed maximum. For models that yield $R > 48$ km (or even > 50 km, for that matter), the fits are not even marginally “good.”

Others report nuclear radii that fall within the range 20 to 30 km: e.g., Wink (1999) from millimeter-continuum measurements, and Fernández *et al.* (in preparation) from centimeter and mid-infrared continuum measurements. Optical measurements of the nuclear cross section (via *HST* WFPC2 imaging) yield comparable values (using the standard assumptions of geometric albedo, p , of 0.04 and a linear phase coefficient, β , of 0.035 mag/deg), but appear to depend heavily on the analysis method; e.g., note the differing results reported by Weaver *et al.* (1997), Fernández *et al.* (in preparation), and Sekanina (1999) based on the same images.

It should be emphasized that we have not modeled an aspherical nucleus; all our results assume sphericity.

c. Inner Coma: Albedo of Dust Grains

Since we have measured the opacity of the coma, we can calculate the albedo of the dust in the inner coma by using measured values of $Af\rho_o$ (introduced by A'Hearn *et al.* 1984), where A is the albedo, f is the filling factor, and ρ_o is the size at the comet of the aperture used. It is obtained via

$$Af\rho_o = \frac{F_{\text{comet}}}{F_{\odot}} \times \left(\frac{r}{1 \text{ AU}} \right)^2 \times \frac{4\Delta^2}{\rho_o}, \quad (4)$$

where r is the heliocentric distance of the comet, Δ is the geocentric distance, F_{\odot} is the solar flux at Earth, and F_{comet} is the comet's flux measured in the aperture. The filling factor is the aperture average of $1 - e^{-\tau(\rho)}$. Here the albedo is properly the value of the scattering function relative to a conservative, isotropic scatterer, as outlined by Hanner *et al.* (1981; and equal to $4\pi\sigma(\theta)/G$ in that work).

We analyzed HST WFPC2 images of the comet obtained 12 days before and 12 days after the occultation event (provided by H. A. Weaver of Johns Hopkins University), and $Af\rho_o$ was measured down to a cometocentric distance of 400 km (about 0.2 arcsec). A steady-state, force-free, radially flowing dust coma would have an aperture-independent value of $Af\rho_o$, but since Hale-Bopp's coma was not like this, we extrapolated $Af\rho_o$ down to 100 km for comparison with our occultation results. Since the phase angle of the observations was only 19° , we removed the phase angle effect, $\phi(\alpha)$, by using

$$\phi(\alpha) = 10^{-0.4\alpha\beta}, \quad (5)$$

where β is the phase coefficient of 0.025 mag/degree (a value roughly consistent across several comets; Meech and Jewitt 1987), and α is the phase angle at the time of the observation. We estimate that $Af\rho_o/\phi(\alpha)$ was about 1.3 ± 0.3 km on 23 Sep 1996 and 1.9 ± 0.3 km on 17 Oct 1996. Time variability of the comet's flux in the HST images leads to the large error estimates. Taking $Af\rho_o/\phi(\alpha) = 1.6 \pm 0.3$ km on 5 Oct 1996, $\rho_o = 100$ km, and the aperture average of $1 - e^{-\tau}$ to be about 0.38 ± 0.05 , we find $A/\phi(\alpha)$ to be 0.04 ± 0.01 (formal error). This leads to an equivalent geometric albedo, p , of $\frac{1}{4}A/\phi(\alpha) = 0.01 \pm 0.002$. This value is rather low (e.g., Divine *et al.* (1986) collate information from various workers to obtain an average p of 0.03 ± 0.01), and a possible explanation (similar to that given by Larson and A'Hearn 1984) is that a photon is doubly scattered by the dust in the inner coma. It is not unreasonable to expect such a scenario in the optically thick portion of the coma. If every photon were doubly scattered, $A/\phi(\alpha)$ would be the square root of the value given above: 0.21 ± 0.02 (formal error), and $p = 0.05 \pm 0.006$. That the calculated albedo is acceptable provides one self-consistent check that our model results—and specifically the high opacity of the coma—make sense.

d. Inner Coma: Plausibility of Findings

Our modeling implies that the column density of dust in the inner coma follows a power law of ρ with an index steeper

than 1.4. This steepness is not evident in large-scale imaging of the comet. The path of the star's ingress followed the edge of one of Hale-Bopp's jets (short line segments in Fig. 6a) that had a surface brightness proportional to $\rho^{-0.86}$; during egress, the path did not follow a jet, and the coma surface brightness was proportional to $\rho^{-1.26}$. However, one can fit just the wings of our occultation lightcurve (i.e., between 100 and 170 km from mid-occultation) and match the profiles from the large-scale imaging. It is only in the central region, within 100 km of the nucleus, where these profiles fail and the density of dust must be a steep function of ρ . Unfortunately the small scale of these properties of the coma are beyond the reach of other Earth-based observations—even HST Planetary Camera imaging would have covered a full 98 km per pixel.

It is possible that we observed the acceleration region of the dust, and that it may have extended ~ 100 km from the nucleus, steepening the dust profile. Gombosi *et al.* (1986), in their review of inner coma dynamics, state that their modeling shows dust still accelerating toward terminal velocity several nuclear radii away from the nucleus, albeit in a model coma with a lower dust-to-gas ratio (χ) and lower r than Hale-Bopp's. A larger χ could extend the coma's acceleration region, but the larger r (lower insolation, lower dust speed) may counter that effect.

A detailed dusty gas-dynamic model of Hale-Bopp's coma is beyond the scope of this paper, but, using estimates of the dust speed v , we can show the steep opacity profile is roughly compatible with the models of Gombosi *et al.* (1986). We note that azimuthal variations in the dust density (not only the acceleration of the dust) can contribute to the measured shape of the dust profile, but a model of such variations would be difficult to constrain owing to a lack of data. Thus we show here only a gross justification of a steep opacity profile. The profile is proportional to $\rho^{-1.7 \pm 0.3}$ or so, which makes $v \propto \rho^{0.7 \pm 0.3}$ (since surface brightness is proportional to $(\rho v)^{-1}$). Let the nucleus' radius be 25 km; we cannot expect the ρ dependence of v to hold all the way to the surface, so we will estimate v at 5 km above it, say $\rho = 30$ km. Assuming the dust is accelerated out to $\rho = 100$ km, v will be about $(100/30)^{0.7} = 2.3$ times smaller.

Now, the terminal velocity v_t of the dust at the time of the occultation was about 0.6 km/s. This is based on (a) v_t at perihelion ($r = 0.9$ AU) being about 1.0 km/s (Schleicher *et al.* 1998a), and (b) $v_t \propto r^{-0.41}$, which is a relation similar to that used for the speed of the gas in the coma (Biver *et al.* 1999). Therefore, at $\rho = 30$ km, $v \approx (0.6 \text{ km/s})/2.3 \approx 0.27$ km/s. Figure 12a of Gombosi *et al.* (1986) shows their model giving a $0.84\text{-}\mu\text{m}$ -wide dust grain a speed of about 0.25 km/s at about 0.2 nuclear radii above the surface—equivalent in this case to $\rho \approx 30$ km. Since there are differences between Hale-Bopp's environment and that used in the model of Gombosi *et al.* (1986), and further their calculated v does not strictly follow $\rho^{0.7}$, this match between v is somewhat coincidental, but it is clear that v is roughly comparable to model calculations.

We noted the high optical depth implied by our modeling. Canonically, comae must be optically thin so that sunlight can

reach the nucleus to drive the sublimation of gas, leading to the production of the dust in a self-regulating manner. However, an optically thick inner coma could be a secondary source for energy, via scattering of sunlight and thermal reradiation, especially if the dust has been superheated, as seems to be the case for Hale–Bopp (Lisse *et al.* 1999a). This problem has been analyzed by others, who have found by various analytic and numerical simulation methods that the energy deposited to the nucleus is a weak function of comatic optical depth, even up to $\tau \sim 2$; reradiation almost compensates (or, in some analyses, overcompensates) for the decrease in sunlight (see, e.g., Salo 1988, Hellmich 1981, Weissman and Kieffer 1981).

An important check is whether a high τ makes sense. We argue that it does, as follows. $Af\rho_o/\phi(\alpha)$, derived above, is 1.6 ± 0.2 km at $\rho_o = 100$ km. At the time of the *Giotto* flyby of Comet 1P/Halley, Schleicher *et al.* (1998b) report that Halley’s $Af\rho_o/\phi(\alpha) = 0.53$ km, and Keller *et al.* (1987) calculate from *Giotto* imaging that the peak opacity of the dust coma, a few kilometers above the surface of the nucleus, was about 0.3. So Hale–Bopp’s $Af\rho_o/\phi(\alpha)$ from Section IV.c was at least three times larger than Halley’s during the flyby. With the two comets’ dust grains having roughly the same albedo, it is clear that it would be not be difficult for Hale–Bopp to have had a peak τ around unity. Furthermore, it is likely that Hale–Bopp’s near nucleus $Af\rho_o/\phi(\alpha)$ was even higher, for the following reason. Our modeling shows the dust opacity profile to be proportional to $\rho_o^{-1.7 \pm 0.3}$ or so, making $Af\rho_o/\phi(\alpha) \propto \rho_o^{-0.7 \pm 0.3}$. This is not strictly true at the higher optical depths, since $f > 1$ is not allowed, but it does imply that $Af\rho_o/\phi(\alpha)$ is higher than the 1.6 km as one travels in from $\rho = 100$ km, so that it is probably more than three times larger than Halley’s when measured near the nucleus’ surface.

V. SUMMARY

We report constraints on the nuclear and comatic properties of Comet Hale–Bopp as implied by our observations of an occultation of a ninth-magnitude star. Except for the special case of Comet Chiron, this would be the first time such an event with so small an impact parameter has been observed. Our observations were marred by thin clouds and a lack of adequate corroborating data—only one chord through a sufficiently thick portion of the coma was apparently measured—but there are many pieces of circumstantial evidence to show that we indeed observed the occultation. Moreover, we know of no other observations of the comet that can disprove our conclusions. Our data nearest the nucleus were collected about 800 km from the latest prediction, but this is not unreasonable since such a distance is comparable to the astrometric error in determining the nucleus’ location within a finitely pixelized image dominated by comatic flux.

By modeling the shape of our lightcurve with a simple coma and spherical nucleus model, and assuming that our observation recorded the occultation, we find the following:

1. Assuming the power-law opacity profile of the coma, with exponent n , is as shallow as or shallower than 2.4, the impact parameter b is ≤ 45 km, but the best fits occur when $b \leq 33$ km. Our occultation observation has sampled the near-nuclear inner coma, which has only rarely been observed before in any comet.

2. If $n \leq 2$, the nucleus is spherical, and the coordinate origin is constrained as depicted in Fig. 4, then the nuclear radius R must be smaller than about 30 km. Relaxing the constraints on n yields an upper limit of 48 km.

3. The inner coma of Hale–Bopp is probably optically thick, even at nearly 3 AU from the Sun. Regardless of the values for the other parameters, good fits to the data can only be found if the opacity within the first few tens of kilometers of the center (not the surface) of the nucleus was at least unity. For some applicable models R is bigger than this distance, in which case the maximum coma opacity is less than one, but never much less.

4. We find that the albedo ($A/\phi(\alpha)$) of the dust while it is within 100 km of the nucleus’ center is 0.21 ± 0.02 (formal error). The equivalent geometric albedo p is 0.05 ± 0.005 (formal error). This assumes that all photons within this region are doubly scattered. Without this caveat, the calculated albedo is lower than the “typical” value ($p = 0.01$, compared to 0.03 from Divine *et al.* 1986).

5. The dust opacity profile is probably steeper than the canonical ρ^{-1} power law, being most likely proportional to ρ^{-n} with $n \geq 1.4$. Marginal fits can be found for $n = 1.0$ for one hemisphere. (The other hemisphere is, in that case, quite steep, $n \approx 2$.) This occurs possibly within 160 or 170 km of the nuclear center, but definitely within 100 km. This chord through the coma may have sampled the acceleration region of the dust, and/or azimuthal variations in the inner coma, so our model, which describes the coma’s density as two hemispheres each having a single power-law function of cometocentric distance, would be too simplistic.

6. The steepness of the profile in the deepest coma does not match that of the jet structure seen in large-scale images, although the resolution of all ground-based imaging fails to directly sample the 100-km scales we are measuring via the occultation. The characteristic n for the wings of the occultation lightcurve could follow the same value as for the large-scale images, and the processes mentioned in Item 5 above may only be important within the first 100 km of the coma.

APPENDIX

The bandpass of Team 5’s system is shown in Fig. A1; all that is needed is the ratio C of star flux to the sum of fluxes from comet, sky, and detector noise within this band and within the 1-arcmin wide aperture that was used. We start with CCD observations of the comet and star taken with the USNOFS 1.5-m telescope on 2, 3, and 5 Oct 1996. We know the relative brightnesses (to $\pm 5\%$) in their passband, the spectral shape of which is also shown in Fig. A1 (Monet *et al.* 1992). To switch to Team 5’s band now requires knowing the spectra of the comet and the star.

Figure A1 shows the spectrum of a typical K0V star (Kharitonov *et al.* 1988, Silva and Cornell 1992, Jacoby *et al.* 1984) and of the Sun (Neckel and Labs 1984, Labs *et al.* 1987). The comet’s spectrum is the same as the solar

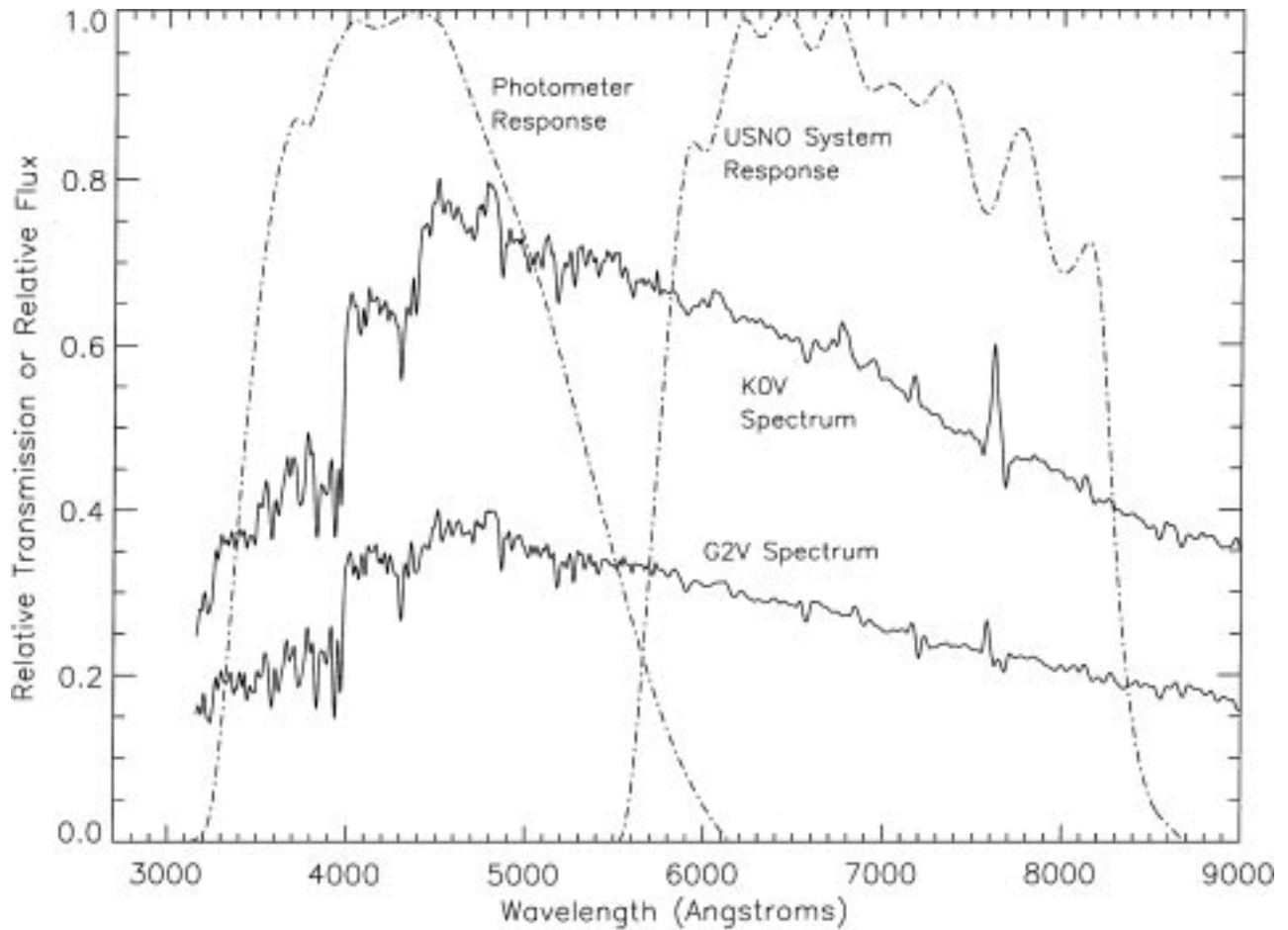


FIG. A1. Comparison of the bandpasses (dashed lines) of the observing system at the USNO 1.5-m telescope and of the C-14 and photometer system used by Team 5 for the occultation. A comparison of the spectra (solid lines) of a K0V star and a solar-type star, which in this case approximates the spectrum of the comet, was used to transform the relative brightnesses of the comet and star from the USNO system to the Team 5 system.

spectrum plus fluorescence emission lines and any reddening of the dust. Using CCD imaging taken on 12 Oct 1996 UT with the Lowell Observatory 1.1-m Hall telescope and narrowband International Halley Watch filters (as described by Vanýsek 1984), we found the dust to be at most only 0.03 ± 0.05 mag redder than the Sun. Moreover we found that CN and C₂ emission (the dominant species in Team 5's spectral range) would contribute only about $6\% \pm 1\%$ of the flux. Hence the solar spectrum in Fig. A1 is actually a good representation of the comet's spectrum. In Oct 1996 the comet had almost constant morphology and magnitude, so there is little error in using images taken 7 days after the occultation.

Thus we can calculate the relative star and comet brightnesses to within a few percent. The only caveat is that the systematic error may be higher if our star is not a typical K0V star. Our remaining task is to account for sky and detector noise contributions. The latter we measured to be negligible compared to that of the sky and the comet. From practice observations under conditions roughly as dark as for the observation of the occultation itself, we found the sky to be about $8\% \pm 2\%$ of the comet's brightness, thus the factor from the spectral analysis should be divided by 1.08 ± 0.02 . The combination of all information yields $C = 0.35 \pm 0.02$.

ACKNOWLEDGMENTS

The authors thank Hal Weaver and two anonymous referees for thorough critiques of earlier versions of this manuscript. We greatly appreciate the assis-

tance of Ron Stone and the U.S. Naval Observatory (Flagstaff Station) for aiding preobservation preparations and for making available to us CCD data from the 1.5-m telescope that we present in this work. We acknowledge the help of Don Yeomans for help with finding accurate positions of the comet before and after the occultation, Alison Sherwin for help with the post-occultation observations, and Jeff Hall for confirming the class of the occulted star. We also recognize the assistance of the Centre de Donnés Astronomiques de Starsbourg. During academic year 1996–1997, R.R.H. was on sabbatical at Lowell Observatory. This work was supported by funding from the National Aeronautics and Space Administration and the National Science Foundation.

REFERENCES

- A'Hearn, M. F. 1988. Observations of cometary nuclei. *Ann. Rev. Earth Planet. Sci.* **16**, 273–293.
- A'Hearn, M. F., D. G. Schleicher, P. D. Feldman, R. L. Millis, and D. T. Thompson 1984. Comet Bowell 1980b. *Astron. J.* **89**, 579–591.
- Belton, M. J. S. 1991. Characterization of the rotation of cometary nuclei. In *Comets in the Post-Halley Era* (R. L. Newburn, Jr., M. Neugebauer, and J. Rahe, Eds.), pp. 691–721. Kluwer Academic, Boston.
- Biver, N., and 22 colleagues 1999. Long term evolution of the outgassing of Comet Hale-Bopp from radio observations. *Earth Moon Planets*, in press.

- Bus, S. J., and 20 colleagues 1996. Stellar occultation by 2060 Chiron. *Icarus* **123**, 478–490.
- Combes, M., J. Lecacheux, Th. Encrenaz, B. Sicardy, Y. Zeau, and D. Malaise 1983. On stellar occultations by comets. *Icarus* **56**, 229–232.
- Divine, N. 1981. Numerical models for Halley dust environments. In *The Comet Halley Dust and Gas Environment* (B. Battrock and E. Swallow, Eds.), pp. 25–30. European Space Agency Scientific and Technical Publications Branch, Noordwijk, The Netherlands.
- Divine, N., and 10 colleagues 1986. The Comet Halley dust and gas environment. *Space Sci. Rev.* **43**, 1–104.
- Dossin, F. 1962. Observation de la diminution d'éclat des étoiles vues à travers la région centrale de la Comète Burnham (1959k). *Ann. l'Observatoire de Haute-Provence* **45**, 30–31.
- Gombosi, T. I., T. E. Cravens, and A. F. Nagy 1985. Time-dependent dusty gasdynamical flow near cometary nuclei. *Astrophys. J.* **293**, 328–341.
- Gombosi, T. I., A. F. Nagy, and T. E. Cravens 1986. Dust and neutral gas modeling of the inner atmosphere of comets. *Rev. Geophys.* **24**, 667–700.
- Gombosi, T. I., K. Szegő, B. E. Gribov, R. Z. Sagdeev, V. D. Shapiro, V. I. Shevchenko, and T. E. Cravens 1983. Gas dynamic calculations of dust terminal velocities with realistic dust size distributions. In *Cometary Exploration* (T. I. Gombosi, Ed.), Vol. 2, pp. 99–111. Central Research Institute for Physics, Hungarian Academy of Sciences, Budapest.
- Hanner, M. S., R. H. Giese, K. Weiss, and R. Zerull 1981. On the definition of albedo and application to irregular particles. *Astron. Astrophys.* **104**, 42–46.
- Hellmich, R. 1981. The influence of the radiation transfer in cometary dust halos on the production rates of gas and dust. *Astron. Astrophys.* **93**, 341–346.
- Jacoby, G. H., D. A. Hunter, and C. A. Christian 1984. A library of stellar spectra. *Astrophys. J. Suppl. Ser.* **56**, 257–281.
- Keller, H. U., and 21 colleagues 1987. Comet P/Halley's nucleus and its activity. *Astron. Astrophys.* **187**, 807–823.
- Kharitonov, A. V., V. M. Tereshchenko, and L. N. Knyazeva 1988. *Spectrophotometric Catalogue of Stars*. Izdatel'stvo Nauka Kazakhskoi SSR, Alma-Ata, Kazakh SSR.
- Labs, D., H. Neckel, P. C. Simon, and G. Thuiller 1987. Ultraviolet solar irradiance measurement from 200 to 358 nm during Spacelab 1 mission. *Sol. Phys.* **107**, 203–219.
- Larson, S. M., and M. F. A'Hearn 1984. Comet Bowell (1980b)—Measurement of the optical thickness of the coma and particle albedo from a stellar occultation. *Icarus* **58**, 446–450.
- Lecacheux, J., W. Thuillot, Th. Encrenaz, P. Laques, D. Rouan, and R. Despiou 1984. Stellar occultations by two comets: IRAS-Araki-Alcock (1983d) and P/IRAS (1983j). *Icarus* **60**, 386–390.
- Lisse, C. M., and 14 colleagues 1999a. Infrared observations of the dust emission from Comet Hale-Bopp. *Earth, Moon, Planets*, in press.
- Lisse, C. M., Y. R. Fernández, A. Kundu, M. F. A'Hearn, A. Dayal, L. K. Deutsch, G. G. Fazio, J. L. Hora, and W. F. Hoffmann 1999b. The nucleus of Comet Hyakutake (C/1996 B2). *Icarus* **140**, 189–204.
- Marconi, M. L., and D. A. Mendis 1983. The atmosphere of a dirty-clathrate cometary nucleus: A two-phase, multifluid model. *Astrophys. J.* **273**, 381–396.
- Marconi, M. L., and D. A. Mendis 1984. The effects of the diffuse radiation fields due to multiple scattering and thermal reradiation by dust on the dynamics and thermodynamics of a dust cometary atmosphere. *Astrophys. J.* **287**, 445–454.
- Meech, K. J. 1999. Physical properties of comets. In *Asteroids, Comets, Meteors '96: Proceedings of the 10th COSPAR Colloquium* (A.-C. Levasseur-Regourd and M. Fulchignoni, Eds.), in press. Pergamon-Elsevier, Oxford.
- Meech, K. J., and D. C. Jewitt 1987. Observations of Comet P/Halley at minimum phase angle. *Astron. Astrophys.* **187**, 585–593.
- Monet, D. G., C. C. Dahn, F. J. Vrba, H. C. Harris, J. R. Pier, C. B. Luginbuhl, and H. D. Ables 1992. U. S. Naval Observatory CCD parallaxes of faint stars. I. Program description and first results. *Astron. J.* **103**, 638–665.
- Neckel, H., and D. Labs 1984. The solar radiation between 3300 and 12500 Å. *Sol. Phys.* **90**, 205–258.
- Reitsemá, H. J., W. A. Delamere, A. R. Williams, D. C. Boice, W. F. Huebner, and F. L. Whipple 1989. Dust distribution in the inner coma of Comet Halley: Comparison with models. *Icarus* **81**, 31–40.
- Röser, S., and U. Bastian 1991. *PPM Star Catalogue*. Astronomisches Rechen-Institut Heidelberg and Spektrum Akademischer Verlag, Heidelberg.
- Saló, H. 1988. Monte Carlo modeling of the net effects of coma scattering and thermal reradiation on the energy input to cometary nucleus [sic]. *Icarus* **76**, 253–269.
- Schleicher, D. G., T. L. Farnham, B. R. Smith, E. A. Blount, E. Nielsen, and S. M. Lederer 1998a. Nucleus properties of Comet Hale-Bopp (1995 O1) based on narrowband imaging. *Bull. Am. Astron. Soc.* **30**, 1063–1064. [Abstract]
- Schleicher, D. G., R. L. Millis, and P. V. Birch 1998b. Narrowband photometry of Comet P/Halley: Variation with heliocentric distance, season, and solar phase angle. *Icarus* **132**, 397–417.
- Sekanina, Z. 1999. A determination of the nuclear size of Comet Hale-Bopp (C/1995 O1). *Earth, Moon, Planets*, in press.
- Silva, D. R., and M. E. Cornell 1992. A new library of optical spectra. *Astrophys. J. Suppl. Ser.* **81**, 865–881.
- Smithsonian Astrophysical Observatory 1966. *Smithsonian Astrophysical Observatory Star Catalog*. Smithsonian Institution, Washington.
- Thomas, N., and H. U. Keller 1987. Comet P/Halley's near-nucleus jet activity. In *Symposium on the Diversity and Similarity of Comets* (E. J. Rolfe and B. Battrock, Eds.), pp. 337–342. European Space Agency Publications Division, Noordwijk, The Netherlands.
- Thomas, N., and H. U. Keller 1990. Interpretation of the inner coma observations of Comet P/Halley by the Halley Multicolour Camera. *Ann. Geophys.* **8**, 147–166.
- Vanýsek, V. 1984. Photometric system for the International Halley Watch. In *Asteroids Comets Meteors* (C.-I. Lagerkvist and H. Rickman, Eds.), pp. 355–358. Astronomiska Observatoriet, Uppsala, Sweden.
- Weaver, H. A., and P. L. Lamy 1999. Estimating the size of Hale-Bopp's nucleus. *Earth, Moon, Planets*, in press.
- Weaver, H. A., P. D. Feldman, M. F. A'Hearn, C. Arpigny, J. C. Brandt, M. C. Festou, M. Haken, J. B. McPhate, S. A. Stern, and G. P. Tozzi 1997. The activity and size of the nucleus of Comet Hale-Bopp (C/1995 O1). *Science* **275**, 1900–1904.
- Weissman, P. R., and H. H. Kieffer 1981. Thermal modeling of cometary nuclei. *Icarus* **47**, 302–311.
- Wink, J. E. 1999. Coordinated observations of Comet Hale-Bopp between 32 and 860 GHz. *Earth, Moon, Planets*, in press.